Atmospheric Environment 106 (2015) 241–251

Contents lists available at ScienceDirect

Atmospheric Environment

journal homepage: www.elsevier.com/locate/atmosenv

Source term estimation using air concentration measurements and a Lagrangian dispersion model – Experiments with pseudo and real cesium-137 observations from the Fukushima nuclear accident

Tianfeng Chai [a, b, *], Roland Draxler [a], Ariel Stein [a]

[a] NOAA Air Resources Laboratory (ARL), NOAA Center for Weather and Climate Prediction, 5830 University Research Court College Park, MD 20740, USA
[b] Cooperative Institute for Climate and Satellites, University of Maryland, College Park, MD 20740, USA

HIGHLIGHTS

- Emission inversion has been built based on a Lagrangian model and a cost function.
- Cs-137 releases from Fukushima accident were recovered using global measurements.
- Using ln(c) differences in the cost function is better than using concentrations.
- Inversion is not sensitive to observational errors or different first guesses.
- A temporal smoothness penalty can remove artificial variability from the results.

ARTICLE INFO

Article history:
Received 5 November 2014
Received in revised form
28 January 2015
Accepted 29 January 2015
Available online 30 January 2015

Keywords:
Lagrangian dispersion model
Fukushima nuclear accident
Cost functional
Source term estimation
Air concentration
Pseudo observations
Hybrid Single Particle Lagrangian Integrated Trajectory (HYSPLIT) model
Transfer coefficient matrix (TCM)
Cesium-137

ABSTRACT

A transfer coefficient matrix (TCM) was created in a previous study using a Lagrangian dispersion model to provide plume predictions under different emission scenarios. The TCM estimates the contribution of each emission period to all sampling locations and can be used to estimate source terms by adjusting emission rates to match the model prediction with the measurements. In this paper, the TCM is used to formulate a cost functional that measures the differences between the model predictions and the actual air concentration measurements. The cost functional also includes a background term which adds the differences between a first guess and the updated emission estimates. Uncertainties of the measurements, as well as those for the first guess of source terms are both considered in the cost functional. In addition, a penalty term is added to create a smooth temporal change in the release rate. The method is first tested with pseudo observations generated using the Hybrid Single Particle Lagrangian Integrated Trajectory (HYSPLIT) model at the same location and time as the actual observations. The inverse estimation system is able to accurately recover the release rates and performs better than a direct solution using singular value decomposition (SVD). It is found that computing $ln(c)$ differences between model and observations is better than using the original concentration c differences in the cost functional. The inverse estimation results are not sensitive to artificially introduced observational errors or different first guesses. To further test the method, daily average cesium-137 air concentration measurements around the globe from the Fukushima nuclear accident are used to estimate the release of the radionuclide. Compared with the latest estimates by Katata et al. (2014), the recovered release rates successfully capture the main temporal variations. When using subsets of the measured data, the inverse estimation method still manages to identify most of the major events in the temporal profile of the release.

1. Introduction

The transport and dispersion of gaseous and particulate pollutants in the atmosphere can be modeled using either Eulerian or Lagrangian approaches. In the Lagrangian approach, a large number of trajectories of "particles" starting from a source location are

* Corresponding author. NOAA Air Resources Laboratory (ARL), NOAA Center for Weather and Climate Prediction, 5830 University Research Court College Park, MD 20740, USA.
E-mail address: Tianfeng.Chai@noaa.gov (T. Chai).

http://dx.doi.org/10.1016/j.atmosenv.2015.01.070

tracked in the atmosphere to predict the transport and dispersion of pollutants. Lagrangian particle dispersion models are frequently employed to provide plume products associated with emergency response scenarios. For instance, the National Oceanic and Atmospheric Administration (NOAA) in the United States has been using the Hybrid Single Particle Lagrangian Integrated Trajectory (HYSPLIT) model (Draxler and Hess, 1998) to provide long-range plume forecasts to World Meteorological Organization (WMO) member states in North, Central, and South America, and the International Atomic Energy Agency (IAEA) when requested since 1993 (Draxler et al., 1993; Rolph et al., 1993).

For dispersion problems with complex emission scenarios, Draxler and Rolph (2012) developed a procedure to model atmospheric radionuclide air concentrations using a transfer coefficient matrix (TCM) generated using a Lagrangian dispersion model. In this procedure, independent simulations are first performed with a unit emission rate from each source location and pre-defined time segment. The time varying model predictions at all receptor locations (or grid points) are tabulated to generate the TCM. The same TCM can repeatedly be used to generate model predictions with different release scenarios. In this approach, each set of input parameters, i.e., a release scenario, is used to compute the deterministic set of predictions at all receptors, subject to model error and uncertainties.

In many situations the actual emissions may be difficult to obtain quickly, such as during nuclear accidents, volcanic eruptions, and wild fires. Inverse modeling approaches are often employed to utilize observations and numerical models to estimate the emissions. The linearity of the Lagrangian dispersion model is inherent to the TCM approach. The transfer coefficients in the TCM contain the sensitivities of the receptors with respect to all emission terms as calculated by the Lagrangian dispersion model and do not need to be repeated again for different emission scenarios. If there are enough measurements, the emission rates can be directly solved using singular value decomposition (SVD). However, potential problems (e.g., singularities) may arise when the uncertainty of the dispersion model and observations are not carefully considered. Solving the inverse problem under a general variational data assimilation framework allows many uncertainty parameters and heterogeneous types of measurements to be formulated into a single cost functional (e.g., Winiarek et al., 2014). In theory, the solution that minimizes the cost functional provides the best estimate of the release scenario.

The release of radioactive materials from the Fukushima Daiichi Nuclear Power plant accident resulting from the earthquake and tsunami in March 2011 has been estimated using various methods. Chino et al. (2011) gave a first preliminary estimation of release amounts of iodine-131 (I-131) and cesium-137 (Cs-137) into the atmosphere from the accident by coupling environmental monitoring data in Japan with dispersion simulations. The temporal emission variation of the release was later updated by Katata et al. (2012) and Terada et al. (2012) with additional regional monitoring data. Katata et al. (2014) provided the latest update of their reverse and inverse estimation results after adding an oceanic dispersion model and further refinement of the deposition scheme. The radionuclides released after the accident were detected at monitoring stations worldwide, including those of the International Monitoring System (IMS) to support the Comprehensive Nuclear-Test-Ban Treaty (CTBT) (Auer and Prior, 2014). Schöeppner et al. (2012), Stohl et al. (2012), and Achim et al. (2014) estimated the source terms using global monitoring data. Among the attempts to estimate the Fukushima radiation release employing atmospheric dispersion model and monitoring data, many obtained results directly based on the simple comparison between model outputs and measurements (e.g. Chino et al., 2011; Katata et al., 2012; Terada et al., 2012; Hirao et al., 2013; Kobayashi et al., 2013; Oza et al., 2013; Katata et al., 2014; Achim et al., 2014), while others used a more formal inverse modeling approach by introducing a cost functional and *a priori* estimate (e.g. Stohl et al., 2012; Winiarek et al., 2012; Saunier et al., 2013; Winiarek et al., 2014).

The main purpose of this study is to determine whether global monitoring networks, such as the IMS of CTBT can be used to quantify temporal variations of emissions from a known source location, using the Fukushima accident as a case study. The IMS observations were previously used in source region estimation (Becker et al., 2007), which is related but different from our objective here. In the studies to estimate the Fukushima source terms, both Stohl et al. (2012) and Achim et al. (2014) included close-in observations at finer temporal resolutions in addition to the global measurements. Our assumption is that close-in observations would not generally be available in typical CTBT applications. Schöeppner et al. (2012) used observations from three CTBT stations and their respective source-receptor sensitivities to obtain three sets of time-dependent source-terms based on data from each station separately. By introducing a cost functional, we consider the observations from many stations simultaneously. Compared to the previous studies that also introduced a cost functional and *a priori* estimate (e.g. Stohl et al., 2012; Winiarek et al., 2012; Saunier et al., 2013; Winiarek et al., 2014), a more detailed sensitivity study is provided to validate the assumptions of our inverse estimation technique.

In this study, the TCM is used to formulate a cost functional that contains three terms: an observational term calculating the differences between the model predictions and the actual air concentration measurements; a background term measuring the deviation of the solution from the first guess; and a smoothness term penalizing abrupt changes in the temporal profile of the release rate. The best estimate of the release rates is found by minimizing the cost functional using an optimization routine. Uncertainties of the measurements, as well as those for the first guess of source terms are formally considered in the cost functional formulation.

The paper is organized as follows. Section 2 describes the methodology of the inverse modeling, as well as a brief introduction of the HYSPLIT model and the TCM approach. Section 3 presents test cases with pseudo observations generated using the HYSPLIT model. Estimates of the Cs-137 release using actual air concentration measurements from the Fukushima nuclear accident are presented and discussed in Section 4. A summary is given in Section 5.

2. Methodology

2.1. HYSPLIT model and configuration

In this study, the transport and dispersion of the radionuclide Cs-137 are modeled using a Lagrangian approach with the HYSPLIT model. In HYSPLIT, a large number of particles, which are considered computational “point” entities that may be particles or gases, are released at the source location and passively follow the wind. A random component is added to the mean advection velocity in each of the three-dimensional wind component directions to simulate the dispersion of pollutants. The vertical and horizontal turbulence is computed from the local stability estimated from the wind and temperature profiles. Air concentrations, or dispersion factors in this case, are computed by summing each particle's mass as it passes over a concentration grid cell and dividing the result by the cell's volume. A detailed description of the computational aspects of the model can be found in Draxler and Hess (1997, 1998).

All calculations used the 0.5-degree horizontal resolution

meteorological data from NOAA's Global Data Assimilation System (GDAS) (Kleist et al., 2009), consisting of a series of 0 to +6 h forecasts available on 56 native model sigma levels with meteorological fields available every three hours. In the HYSPLIT simulation, Cs-137 is treated as a particle, with a small dry deposition velocity of 0.001 m/s. The original HYSPLIT calculations (Draxler and Rolph, 2012) for the Fukushima accident used a particle release rate of only 5000 per hour. In subsequent calculations, the particle release rate was increased to 20,000 per hour. Further increasing the release rate to 100,000 per hour has little effect on either the HYSPLIT model simulation or the inverse emission estimates. In all previous simulations, the wet deposition was divided into within- and below-cloud scavenging. The within-cloud scheme was based upon an empirically derived scavenging ratio based on the ratio of pollutant concentration measurements in rain to air, while the below-cloud process was parameterized through a decay process defined by a time constant. The revised scavenging scheme used here is a simplified version of the previous scheme using the same time constant decay process for both within- and below-cloud removal. The numerical formulation is the same as in the NAME model (Maryon et al., 1999; Sportisse, 2007), where $B = AR^{0.79}$ and the base scavenging $A = 8 \times 10^{-5}\ s^{-1}$ for particulate Cesium, with the rainfall rate R given in $mm\ h^{-1}$. Radioactive decay is applied in the post-processing step, when converting the TCMs to air concentration, but it has little effect on the Cs-137 results because of its long half-life (~30.17 years). The air concentration grid is global at 1-degree horizontal resolution with a vertical extent of 500 m. The relatively coarse concentration grid restricted the application of the TCM to more distant samplers rather than any close-in measurements, but permitted the use of fewer particles for each simulation.

2.2. Cs-137 sampling data

In this paper, the Cs-137 air concentration sampling data are derived from three public sources: the U.S. (www.usandc.gov/radionuclide.html) and Canadian (www.hc-sc.gc.ca/hc-ps/ed-ud/respond/nuclea/data-donnees-eng.php) CTBT IMS, various European national networks (Masson et al., 2011), and the U.S. EPA (www.epa.gov/japan2011/rert/radnet-sampling-data.html). Hereafter they are referred as CTBT, EURO, and EPAR data. The extra measurements used by Draxler and Rolph (2012) are denoted as "EXTR" and are included in the study as well. Sampling data with higher temporal resolutions are converted into 24-h average concentrations in the paper to follow the CTBT sampling protocols (Becker et al., 2007). Table 1 lists the number of monitoring stations and total number of samples from each data source. The distribution of the measuring stations are shown in Fig. 1. Europe was well monitored by a densely located network, but it took seven days for the polluted air to reach the area before it was detected (Masson et al., 2011). All the monitoring stations listed here are far away from the source at the Fukushima Daiichi nuclear power plant. When estimating the source strength from measurements, local observations dominated the results. Our intent is to examine whether a global monitoring network alone can be used to quantify the emissions.

Table 1
List of Cs-137 air concentration sampling data. Numbers in "()" show the counts of stations and samples before certain data are excluded. Four observation records at Dutch Harbor, Alaska site in the EPAR and seven records at Dublin/Belfield site in the EURO data are excluded because they are already included in the EXTR data sets. The other excluded samples, four from CTBT, five from EURO (including a lone sample data point from Roma), and two from EXTR, are not affected by any of the releases in the current HYSPLIT simulation.

Data source	Number of monitoring stations	Count of total samples
CTBT	14	417 (421)
EPAR	19 (20)	35 (39)
EURO	78 (80)	785 (797)
EXTR	4	59 (61)
Total	115 (118)	1296 (1318)

2.3. Transfer coefficient matrix (TCM)

The transfer coefficients in the TCM are essentially air concentrations resulting from dispersion computation using a unit emission rate. For this Fukushima case study, the time period from 18Z on March 11, 2011 to 12Z on April 5, 2011 is divided into 99 continuous segments of six hours. An independent simulation is then conducted for each segment, in which an emissions rate of 1 unit/h is utilized only for the designated 6-h segment, with zero emissions at all other times. All 99 independent simulations continue through 20 April, 2011 to cover the sampling time period for the last measurement considered in this study. For each simulation, three-dimensional (3-D) 6-h average concentration fields are output at 6-h intervals. The transfer coefficients are thus obtained in the following form as described in Draxler and Rolph (2012).

$$TCM_{ijk} \tag{1}$$

where i indicates the release segment, j denotes the sampling time period, and k is the grid index.

Model concentration c_{jk}^{h} at sampling time "j" and grid point "k" is calculated as

$$c_{jk}^{h} = \sum_{i} q_i \cdot D \cdot TCM_{ijk}, \tag{2}$$

where q_i is the emissions rate (assumed constant) during the ith 6-h release segment. The superscript "h" denotes predictions from HYSPLIT model. Later in text the observed concentrations are given the superscript "o" to differentiate between model predictions and observations. D is the radioactive decay factor. The sum is taken over all release time periods. To reconstruct model-calculated air concentrations, temporal and spatial interpolation may be needed. In the current study, the grid point covering the measurement site is directly used without spatial interpolation. For the 24-h sampling data, the average of four c_{jk}^{h} 6-h concentrations are taken as the model counterpart. For simplicity in notation, the sampling time "j" and the spatial location "k" are combined into one index "m" to represent an independent sampling data point, analogous to our use of a single index "k" to denote a grid point in a 3-D space. That is,

$$c_{m}^{h} = \sum_{i} q_i \cdot H_{im}, \tag{3}$$

where H_{im} is $D \cdot TCM_{ijk}$ with additional temporal and spatial interpolation considered when necessary. Fig. 2 illustrates the average H_{im} values at the 115 stations and with respect to the 99 release segments.

2.4. Singular value decomposition (SVD) approach

In the singular value decomposition (SVD) approach, a matrix pseudo-inverse obtained using its singular values and associated singular vectors is used to directly construct the solution of a overdetermined linear system. When all M measurements are considered at the same time, the model counterparts $(c_1^h, \cdots, c_M^h)^T$ can be

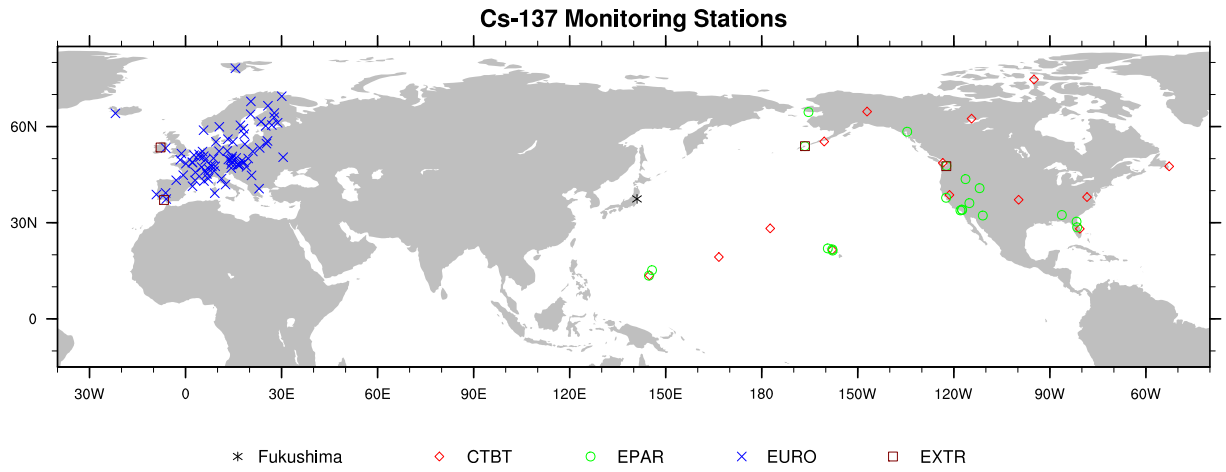

Fig. 1. Distribution of Cs-137 monitoring stations.

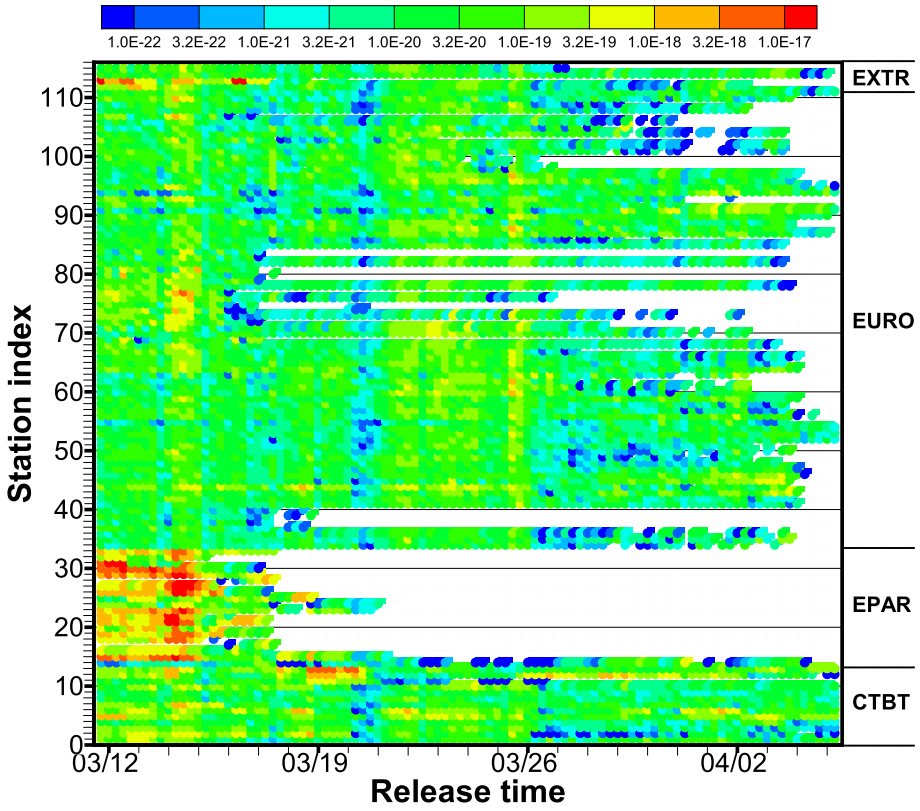

Fig. 2. Average H_{im} values at 117 stations and 99 release segments. Station indices for each data sets are, CTBT: 1–14, EPAR: 15–33, EURO: 34–111, EXTR: 112–115. Blank spots indicate zero H_{im} values for all measurements at the station, corresponding to the release segment "i". Units of H_{im} are hr/m^3.

written as

$$\begin{pmatrix} c_1^h \\ c_2^h \\ \vdots \\ c_M^h \end{pmatrix} = \begin{pmatrix} H_{1,1} & H_{1,2} & \cdots & H_{1,N} \\ H_{2,1} & H_{2,2} & \cdots & H_{2,N} \\ \vdots & \vdots & \ddots & \vdots \\ H_{M,1} & H_{M,2} & \cdots & H_{M,N} \end{pmatrix} \begin{pmatrix} q_1 \\ q_2 \\ \vdots \\ q_N \end{pmatrix} \tag{4}$$

where N is the number of release segments. Assuming that the dispersion model is accurate enough, having enough independent measurements ($M \gg N$) allows the emission rates be directly solved with a SVD solver. When there are less than N independent measurements, the problem becomes under-determined. It will be shown later that the straightforward SVD approach is extremely sensitive to observational error even when the problem is well-defined with ($M \gg N$).

2.5. Formulation of the inverse problem

In general, an inverse problem can be naturally formulated under a variational data assimilation framework. The solution is found by minimizing a cost functional that integrates the differences between model predictions and observations, deviations of

the final solution from the first guess (*a priori*), as well as other relevant information written into penalty terms (Daley, 1991). Such formulation allows heterogeneous types of measurements to be considered simultaneously and the uncertainty to be treated in a statistically rigorous way. For the current problem, the cost functional $\mathscr{J}$ is defined as,

$$\mathscr{J} = \frac{1}{2}\sum_{i=1}^{N}\frac{\left(q_i - q_i^b\right)^2}{\sigma_i^2} + \frac{1}{2}\sum_{m=1}^{M}\frac{\left(c_m^h - c_m^o\right)^2}{\varepsilon_m^2} + \frac{c_{sm}}{2}\cdot\sum_{i=2}^{N-1}\left[\frac{\left(q_{i-1} - q_{i-1}^b\right) - 2\cdot\left(q_i - q_i^b\right) + \left(q_{i+1} - q_{i+1}^b\right)}{q_c}\right]^2 \quad (5)$$

where N = 99, and M = 1296 for the current setup when all Cs-137 measurements listed in Table 1 are used. The control vector $[q_1,\cdots,q_N]$ describes the release scenario and it will be solved through the minimization of the cost functional. The first guess $[q_1^b,\cdots,q_N^b]$ of the control vector is often called the background estimate in data assimilation. We assume the uncertainties of the release at each segment are independent of each other so that only the diagonal term of the typical background error variance σ_i^2 appears in Equation (5). The observational errors are also assumed to be uncorrelated. ε_m^2 are the variances of the observations and representative errors can also contribute to this term. Because it is difficult to verify whether the temporal changes of Cs-137 releases are realistic or not, a smoothness penalty term is added to minimize abrupt changes of q_i. This penalty term also helps to make the modified minimization problem better conditioned (Lin et al., 2002). c_{sm} is a coefficient used to adjust the smoothness of the final solution. It is set to zero for all the twin experiments discussed in the next section. q_c is a scale constant, given as $q_c = 10^{12}$ *Bq/h* in the following applications. A large-scale bound-constrained limited-memory quasi-Newton code, L-BFGS-B (Zhu et al., 1997) is used to minimize the cost functional $\mathscr{J}$ defined in Equation (5).

3. Twin experiments

Twin experiments in which pseudo-observations are generated using the same model as for the inverse calculation are first conducted to answer some basic questions on the source estimation problem. For the current application, a pseudo-observation vector

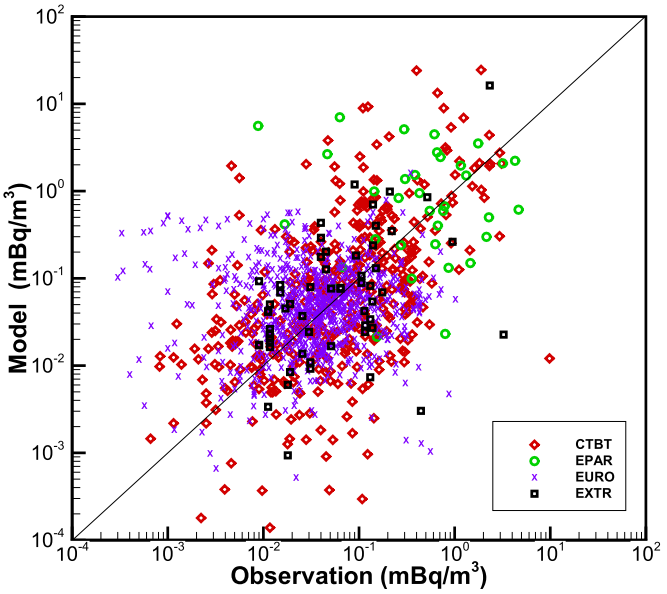

Fig. 4. Scatter plot of the simulated Cs-137 and observations. Cs-137 release estimates by Katata et al. (2014) shown in Fig. 3 are used in the HYSPLIT model simulation.

$\mathbf{c}^p$ is obtained using Equation (6) where the previously computed **H** replaced the need to re-run the HYSPLIT model.

$$\mathbf{c^p} = \mathbf{H}\cdot\mathbf{q} + \varepsilon \quad (6)$$

In Equation (6), "p" denotes pseudo-observations. The pseudo-observations are generated at the same location and time as the real observations listed in Table 1. All 1296 pseudo-observations are used in the following twin experiments. The latest estimates of Cs-137 releases provided by Katata et al. (2014) are used for **q**. Fig. 3 shows the Katata et al. emission estimates, as well as those by Stohl et al. (2012). ε is a vector added to simulate the observational errors calculated as,

$$\varepsilon_m^p = \left(f_m^p \times c_m^p + a_m^p\right) \times r_m, \quad m = 1,\cdots,M, \quad (7)$$

where r_m is a random number drawn from a normal distribution with zero mean and unit variance applied to the mth pseudo-

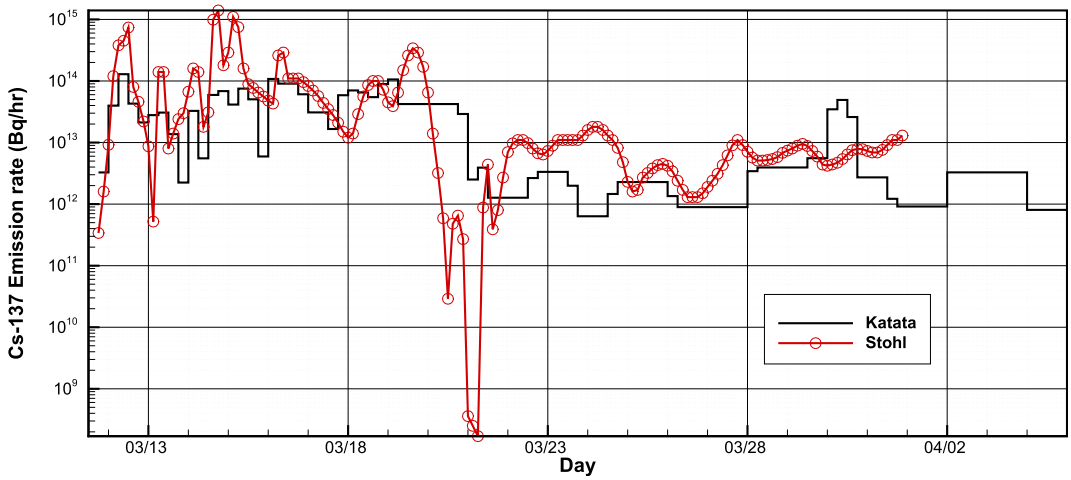

Fig. 3. Temporal variations of the Cs-137 releases. "Katata" estimates at 6-h segments are converted from the latest estimates by Katata et al. (2014). "Stohl" estimates at 3-h segments are *a posteriori* results by Stohl et al. (2012).

observation. The magnitude of the variance is composed of a fractional component $f_m^p \times c_m^p$ and an additive part a_m^p. For the EURO Cs-137 samples, the median of fractional errors for 671 records is 10% and 0.003 mBq/m^3 is the median of 23 absolute errors provided for the other records.

3.1. Control and metric variables

To minimize the cost functional defined in Equation (5), the control variables can be changed to $[ln(q_1),\cdots,ln(q_N)]$ so that the solution belongs to $\mathbb{R}^N$ instead of $\mathbb{R}^N_{\geq 0}$. On the other hand, when comparing model results with observations, $(c_m^h - c_m^o)$ in Equation (5) can be replaced with $ln(c_m^h) - ln(c_m^o)$. In fact, the model simulation errors are found to be close to a log-normal distribution. Adding the logarithmic operation over the concentration helps satisfy the underlying assumption of the normal distributions for the differences between model and observation in variational data assimilation. In addition, Figs. 3 and 4 display wide ranges of Cs-137 release rates and air concentration measurements. The logarithmic operation of a variable with large ranges will also improve the conditioning of the minimization problem.

When $[ln(q_1),\cdots,ln(q_N)]$ is taken as the control vector, switching between q and ln(q) is only needed right before and after calling the L-BFGS-B routine. The gradient vector elements can be calculated using the following formula,

$$\frac{\partial \mathscr{F}}{\partial ln(q_i)} = \frac{\partial \mathscr{F}}{\partial q_i} \cdot \left[\frac{\partial ln(q_i)}{\partial q_i}\right]^{-1} = q_i \cdot \frac{\partial \mathscr{F}}{\partial q_i}, \quad i = 1, \cdots, N. \tag{8}$$

If ln(c) is used as the metric variable, i.e., $ln(c_m^h) - ln(c_m^o)$ is used to calculate the differences between model and observations, $\varepsilon_m^{ln(c)}$ can be simply calculated from ε_m^c as

$$\varepsilon_m^{ln(c)} = f_m^c + \frac{a_m^c}{c_m}, \tag{9}$$

where f_m^c and a_m^c denote the fractional and additive parameters used to calculate the measurement errors in its original concentration form (ε_m^c).

Table 2 lists the test cases with different arrangements of control and metric variables. Noise is not added to the pseudo observations in cases T01-04 to avoid the complication of sensitivity to observational errors. When solving the minimization problem, the uncertainties of the observations are assumed to be small: $\varepsilon_m^c = 0.001 \times c_m^p + 3 \times 10^{-5} mBq/m^3$, i.e., 1% of its typical values found for the EURO data. A constant first guess emission rate of 10^{13} Bq/hr throughout the release period is given with large uncertainties of $\sigma_i = 10^5 \times 10^{13} + 10^9 \approx 10^{18} Bq/hr$. A constraint of $q \geq 10^{11}$ is given to the L-BFGS-B routine as the lower bounds when q is chosen as the control variable. No bounds are needed when $ln(q)$ is taken as the control variable. An optimization solution is considered found when the cost functional is reduced to be less than 10^{-6} of its original value or the cost functional change between two iterations is smaller than 10^{-13}. The maximum iteration number for L-BFGS-B is set as 500 considering the fact that there is no need to run the dispersion model and the small cost to compute the air concentration with any adjusted release $[q_1,\cdots,q_N]$.

With pseudo-observations generated from a known release scenario for the identical twin experiments, it is easy to evaluate both the release solution and its corresponding Cs-137 concentration predictions. Table 3 shows mean absolute error (MAE), root-mean-square error (RMSE), mean relative error (MRE), and correlation coefficient (R) for both Cs-137 concentrations and release rates. Equation (10) shows MRE formulas, in which q^t denotes the "true" release estimates which are used to generate the pseudo-observations.

$$MRE_c = \frac{1}{M}\sum_{m=1}^{M}\frac{c_m - c_m^p}{c_m^p}$$
$$MRE_q = \frac{1}{N}\sum_{i=1}^{N}\frac{q_i - q_i^t}{q_i^t} \tag{10}$$

The Cs-137 pseudo-observations are nearly perfectly reconstructed for cases T01-04, with a correlation of $R = 1.000$ between the observations and the final model predictions. The MRE for the Cs-137 concentrations ranges from 0.001 for cases T02 and T04 and the worst 0.043, for case T03, but still a small value. Fig. 5 shows the recovered Cs-137 release rates and the Katata release estimates. Cases T04 and T02 are very close to the exact solution. The release rates for the early days are well recovered for all the cases, but the results after March 21 are not as good for cases T01 and T03. This can be explained by the relatively lower sensitivities of the observations with respect to the releases for the later days as shown in Fig. 2. The better performances of cases T02 and T04 which compare the differences of $ln(c)$ than cases T01 and T03 which use the concentrations in Equation (5), suggests that choosing $ln(c)$ as the metric variable is beneficial when the observations of the original variable shows a wide range. Similarly, when the control variable varies drastically, it is helpful to change the control variable as well. The statistics shown in Table 3 indicates that case T04 performs slightly better than case T02. Hereafter, we choose $ln(q)$ and $ln(c)$ as control and metric variables respectively for the subsequent tests.

As discussed earlier, the inverse problem can be directly solved via the SVD approach. Using the same pseudo-observations for cases T01-04, the SVD results are also presented in Table 3 and Fig. 5. Note that there are 22 negative release rates present in the results from the standard SVD routine using double precision (Press et al., 1986). The negative release rates are replaced with zero emissions when calculating the model results. Table 3 indicates that the SVD approach generates reasonable results, but worse than most of the cases using the minimization inverse modeling approach. The SVD results are comparable to those from case T03 which is the worst among T01-04. The recovered releases after March 21 fail to show the temporal variation and almost totally miss the peak on March 30. However, the SVD approach performs quite well for the releases before March 21 and captures the basic patterns albeit having large errors at certain points, for instance, on March 15.

Table 2
List of the twin experiments, *i.e.*, inverse cases using pseudo Cs-137 observations. x is the control variable to be adjusted. y is the metric variable used to calculate the differences between model and observations. f_m^p and a_m^p are the fractional and additive constants used in Equation (7) for the 1296 pseudo-observations. $\epsilon_m = f_m^c \times c_m + a_m^c$ and $\sigma_i = f_i^q \times q_i + a_i^q$ represent uncertainties of the observations and the *a priori* releases, respectively. q^b is the first guess of the control variable. q_{min} is the lower bound of the control variable for the L-BFGS-B routine. Units for concentrations and emission/release rates are mBq/m^3 and Bq/h, respectively.

Case	x	y	f_m^p	a_m^p	f_m^c	a_m^c	f_i^q	a_i^q	q^b	q_{min}
T01	q	c	0	0	0.001	10^{-5}	10^5	10^9	10^{13}	$2\cdot10^{11}$
T02	q	ln(c)	0	0	0.001	10^{-5}	10^5	10^9	10^{13}	$2\cdot10^{11}$
T03	ln(q)	c	0	0	0.001	10^{-5}	10^5	10^9	10^{13}	None
T04	ln(q)	ln(c)	0	0	0.001	10^{-5}	10^5	10^9	10^{13}	None
T05	ln(q)	ln(c)	0.05	0.003	0.10	0.003	10^3	10^{11}	10^{13}	$2\cdot10^{11}$
T06	ln(q)	ln(c)	0.10	0.003	0.10	0.003	10^3	10^{11}	10^{13}	$2\cdot10^{11}$
T07	ln(q)	ln(c)	0.20	0.003	0.10	0.003	10^3	10^{11}	10^{13}	$2\cdot10^{11}$
T08	ln(q)	ln(c)	0.10	0.003	0.10	0.003	10^3	10^{11}	10^{12}	$2\cdot10^{11}$
T09	ln(q)	ln(c)	0.10	0.003	0.10	0.003	10^3	10^{11}	10^{14}	$2\cdot10^{11}$

Table 3
Evaluation statistics of Cs-137 concentrations and recovered releases from the twin experiments. MAE: mean absolute error; RMSE: root-mean-square error; MRE: mean relative error; R: linear correlation coefficient. Units of MAE and RMSE: mBq/m^3 for concentrations, Bq/h for releases.

Case	Cs-137 concentration				Cs-137 release			
	MAE	RMSE	MRE	*R*	MAE	RMSE	MRE	*R*
T01	0.001	0.001	0.008	1.000	0.90×10^{12}	1.88×10^{12}	0.229	0.998
T02	0.000	0.001	0.001	1.000	0.11×10^{12}	0.61×10^{12}	0.012	1.000
T03	0.002	0.004	0.043	1.000	3.32×10^{12}	7.66×10^{12}	0.740	0.965
T04	0.000	0.002	0.001	1.000	0.03×10^{12}	0.08×10^{12}	0.011	1.000
SVD	0.002	0.004	0.035	1.000	3.57×10^{12}	9.06×10^{12}	0.588	0.952
T05	0.027	0.242	0.194	0.995	5.21×10^{12}	9.10×10^{12}	0.720	0.960
S05	0.021	0.091	0.197	0.998	14.37×10^{12}	26.73×10^{12}	2.818	0.699
T06	0.038	0.334	0.310	0.985	5.58×10^{12}	9.19×10^{12}	0.792	0.957
S06	0.051	0.176	0.435	0.993	26.35×10^{12}	50.75×10^{12}	5.386	0.437
T07	0.055	0.433	0.411	0.952	6.67×10^{12}	12.75×10^{12}	0.887	0.907
S07	0.141	0.640	1.020	0.985	50.83×10^{12}	97.82×10^{12}	10.720	0.233
T08	0.038	0.331	0.309	0.985	5.68×10^{12}	9.43×10^{12}	0.800	0.954
T09	0.038	0.334	0.310	0.985	5.58×10^{12}	9.18×10^{12}	0.791	0.957

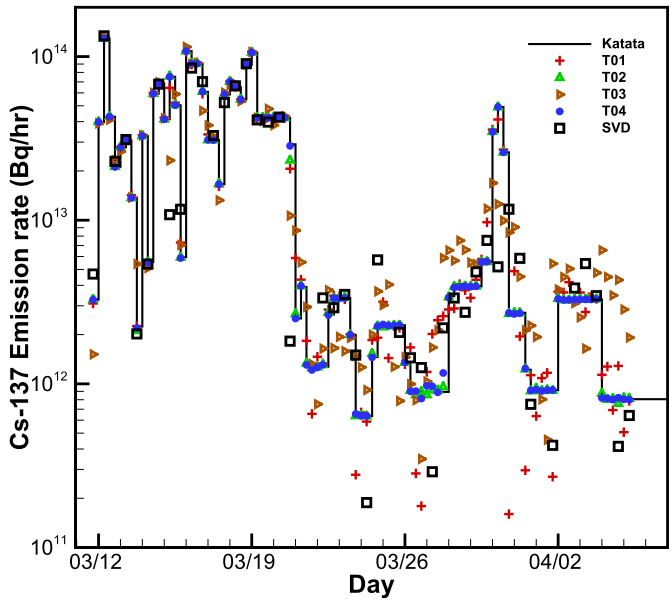

Fig. 5. Cs-137 release estimates from twin experiments T01-04 and solution using singular value decomposition (SVD). Cs-137 release estimates by Katata et al. (2014) are shown for comparison.

3.2. Observation uncertainty

To simulate observational errors, random noise generated using Equation (7) is added to the previous pseudo-observations for Cases T05-07. As listed in Table 2, the fractional components of the errors (f_m^p in Equation (7)) are given as 5%, 10%, and 20% for T05, T06, and T07, respectively. In all three cases, the additive component of the uncertainty (a_m^p in Equation (7)) is assumed constant at 0.003 mBq/m^3. The parameters for observation and *a priori* release uncertainties provided to solve the inverse problem are also modified to be realistic, as shown in Table 2. Note that the observational uncertainty of 10% is kept constant for Cases T05-07 as estimating such parameters is difficult and is primarily determined by the sampling network characteristics.

For the three sets of pseudo-observations, the SVD method is also applied and the evaluation statistics of the results are listed in Table 3. The cases are denoted with "S" followed with the same number as the regular twin tests using the same pseudo-observation set. Because the SVD method only tries to match the observations without any consideration of whether the release solutions are reasonable or not, negative release rates are found for all three cases. The negative release rates are reset to zero when evaluating the concentration statistics. It is not surprising to see good concentration statistics for the SVD cases. However, the release rate results by the SVD method are much worse than cases T05-07. The correlation coefficients for T05-07 are all greater than 0.900, while those for S05-07 are less than 0.700. The MAEs and RMSEs of the releases for cases S05-07 are more than twice of those for cases T05-07. Among the twin tests T05-07, the results get slightly worse as greater noise is added to the pseudo-observations. For case T07, the correlation coefficient between the resolved release rates and the true solution is 0.907, still a reasonably good result. It should be noted that the worse results using the SVD approach is caused by the lack of regularization than the technique alone, which basically gives a least squares solution to an over-determined problem.

3.3. First guess

The *a priori* release rates q_i^b in Equation (5) are required to make the inverse problem well defined. However, it is often difficult to obtain a good *a priori* estimate. In tests T01-07, the constant *a priori* release rate of 10^{13} Bq/hr is rather arbitrary. Thus, a large uncertainty factor has to be associated with the first guess in order to reduce the sensitivity of the final solution to the *a priori*. In tests T01-07 $f_i^q = 1000$ signifies a wide range of the release rates. Cases T08 and T09 test the robustness of the eventual release estimates by changing the *a priori* release rates to 10^{12} Bq/hr, and 10^{14} Bq/hr, respectively. The pseudo-observations are identical to those assimilated in case T06, where Gaussian-distributed random noise with standard deviation of $0.1 \times c_m^p + 0.003\ mBq/m^3$ is added. Except for q_i^b, the other parameters used in tests T08 and T09 are identical to those in case T06. The final solutions of the three cases with different first guesses are almost indistinguishable as indicated by their similar evaluation statistics listed in Table 3.

4. Tests using real observations

The numerical twin experiment tests presented in Section 3 demonstrate that the current inverse algorithm is capable of estimating the release rates from a known source location using air concentration observations. The temporal variations can be resolved with reasonable robustness when pseudo-observations are perturbed with random errors of different magnitudes. Furthermore, the results are not sensitive to the first guess of those releases. However, the above conclusion is based on the

assumption of a "perfect" model because the pseudo-observations are generated by the same model with identical physical parameters and the exact same meteorological fields.

Using the HYSPLIT model with the configuration described in Section 2.1 and Cs-137 releases estimates by Katata et al. (2014), the model results are shown in Fig. 4 as a scatter plot compared with the Cs-137 measurements. Fig. 6 shows the ratio of model versus observations as function of the sampling date. The ratios have a range of 0.001–1000, but mostly fall between 0.1 and 10. Note that the EPAR data used in this paper do not include observations in April and late March, which are currently available.

4.1. Smoothness

Case R01 is conducted by directly replacing the pseudo-observations with the actual measurements listed in Table 1 and keeping all the other parameters used in the twin experiment test T06, as listed in Table 4. The maximum iteration number for L-BFGS-B is increased to 10,000 to ensure the stringent minimization criteria are met before reaching the maximum iteration number. The estimates of high release rates ($q_{min} \geq 10^{12}$ Bq/h) before March 21 agree reasonably well with Katata et al. (2014) results, as shown in Fig. 7(a). However, the release estimates display quite abrupt changes from one 6-h segment to the next. Many segments show release rates reaching the prescribed lower limit of $q_{min} = 2 \times 10^{11}$ Bq/h. While dramatic changes are possible for events such as explosions and deliberate venting, in this application the extreme temporal variations caused by the release rates reaching the prescribed lower limit are mostly spurious. Apparently, the algorithm tries to lower release rates at certain segments in order to correct the overestimation of some samples shown in Fig. 6. Such overestimation may be caused by the uncertainties of the meteorological inputs and parameterization of the deposition processes.

To enforce the smoothness penalty terms, we set the smoothness coefficient c_{sm} in Equation 5 to 1.0 and 0.1 in cases R02 and R03, respectively. Fig. 7(b) shows that the smoothness penalty applied in cases R02 and R03 effectively removed the sudden changes in the release rates. With less spurious temporal variations in the releases, both cases R02 and R03 appear to smooth out the Katata et al. (2014) results at 6-h resolution. Centered 24-h and 96-h running averages are calculated for the Katata et al. (2014) results and are shown in Fig. 7(b). A nearly perfect match is found between R02 and 96-h Katata et al. results from March 16 to March 21. Results of case R03 mostly resemble 24-h Katata et al. results.

Table 4
List of inverse cases using actual Cs-137 measurements. c_{sm} is the smoothness coefficient in Equation (5). ln(q) and ln(c) are chosen as control and measuring variables. $\varepsilon_m = 10\% \times c_m + 0.003 mBq/m^3, m = 1, \cdots M$; $q_i^b = 10^{13} Bq/hr, i = 1, \cdots, N$; $\sigma_i = 10^{16} + 10^{11} \approx 10^{16} Bq/hr, i = 1, \cdots, N$.

Case	Assimilated observations	c_{sm}	Final $\mathcal{F}_{sms}/\mathcal{F}_{total}$
R01	All, M = 1296	0	0
R02	All, M = 1296	1.0	0.021
R03	All, M = 1296	0.1	0.020
R04	CTBT, M = 417	1.0	0.012
R05	EPAR, M = 35	1.0	0.053
R06	EURO, M = 785	1.0	0.030
R07	EXTR, M = 59	1.0	0.049

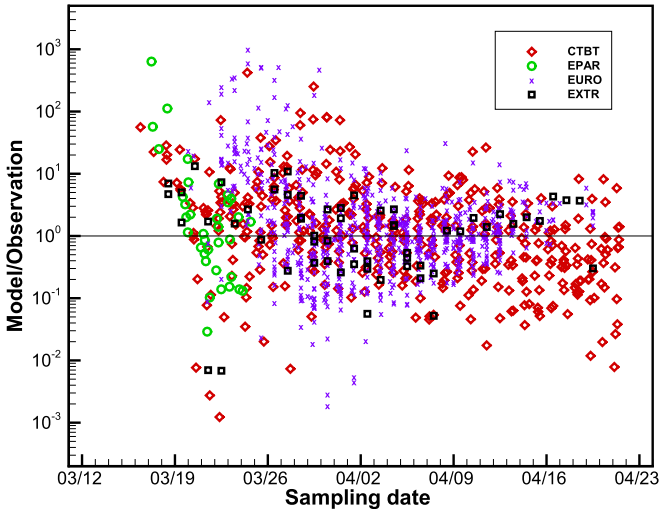

Fig. 6. Ratio of simulated Cs-137 to measurements as a function of observation time using the Cs-137 release estimates by Katata et al. (2014), shown in Fig. 3.

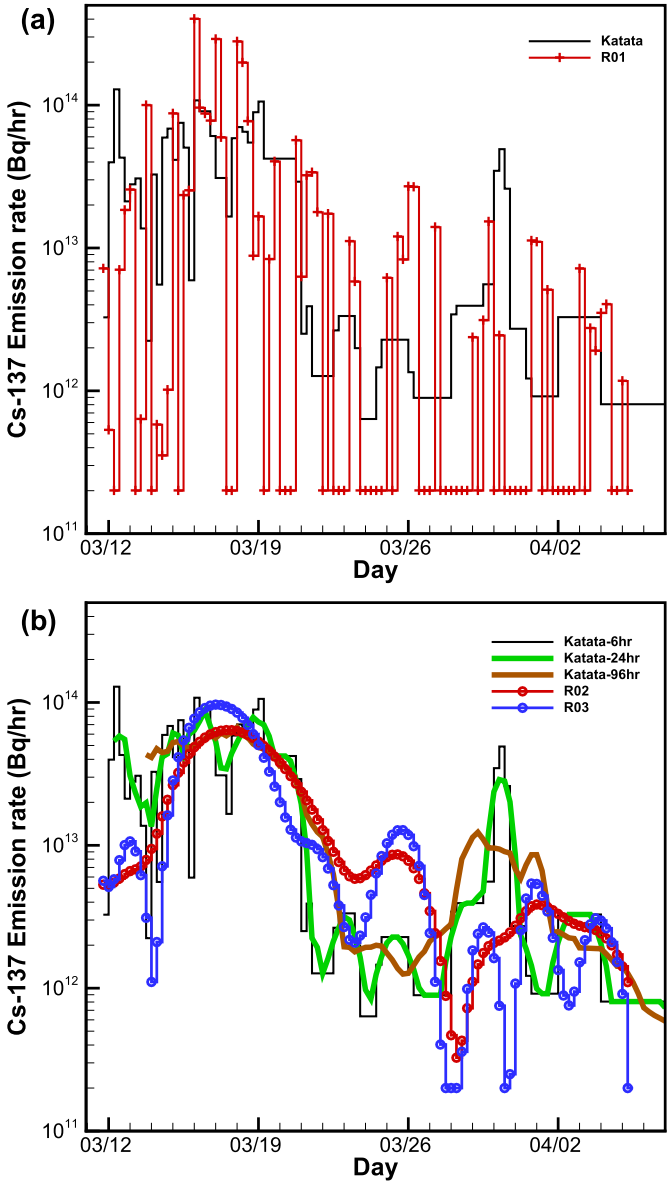

Fig. 7. Cs-137 release estimates from tests using actual measurements without (a) and with (b) smoothness constraints. Cs-137 release estimates by Katata et al. (2014) are also shown for comparison. Katata-24hr and Katata-96hr estimates are centered running averages based on the 6-hr results.

Similar to the twin experiments, the release rates after March 21 are difficult to estimate. All three cases fail to reproduce the peak on March 30–31. The high release rates are possibly due to the core re-melting at Unit 2 on March 30 addressed by Tanabe (2012). Using a high resolution local-scale dispersion model, Katata et al. (2014) showed that the plume turned clockwise from the east to the southwest of the power plant. Wet deposition also occurred over Tochigi and Ibaraki prefectures in the afternoon of March 30 before the plume headed to the ocean. It is difficult for the remote stations to capture the signature of this event. Both R02 and R03 recover a peak release rate between March 25 and 26. The peak coincides with a plateau from March 25 to March 26 in the Katata et al. estimates. The 24-h running averages of their estimates show the peak release at about the same time as what R02 and R03 recover, while 96-h results only give a hint of it a day earlier. Katata et al. (2014) shows another event on March 22. It may reflect the possible core fuel re-melt at Units 3 and 1 on March 21 and March 22–23 speculated by Tanabe (2012). Cases R02-03 results are unable to show this event, but neither are the 96-h Katata et al. results. Clearly, the 96-h running averages smooth out the temporal variations at 6-h resolution and combine several short events into major events visible at lower temporal resolution. Similarly, having smoothness terms in R02 and R03 helps to focus on the major events which are hopeful of being resolved with the current setup using the 24-h observations and a global dispersion model.

Table 5 shows that the correlation between the recovered releases and those by Katata et al. (2014) improved from R = 0.444 for R01 to 0.671 and 0.631 for cases R02 and R03, respectively. Assuming the Katata et al. (2014) estimates as "true" solutions, the MAEs and RMSEs remain large, and the RMEs are close to 100%. The same statistics are calculated for Stohl et al. (2012) estimates shown in Fig. 3. A similar correlation coefficient is found, with $R = 0.512$. However, their results have much larger MAE, RMSE, and RME values, with MAE = 59.6×10^{12} Bq/h, RMSE = 145.3×10^{12} Bq/h, and MRE = 3.51, due to their higher release rates compared to the Katata et al. estimates. The statistics for the Cs-137 concentrations are comparable for cases R01-03, with high MAEs and RMSEs, and low correlation coefficients.

Because we choose $ln(c)$ as metric variables, it might be appropriate to calculate the correlation coefficients based on the $ln(c)$ values for both observation and model results. Such $ln(c)$-based correlation coefficients $R_{ln(c)}$ are also listed in Table 5. $R_{ln(c)}$ for cases R01-03 are 0.518, 0.405, and 0.425, respectively. They are better than their corresponding concentration-based correlation coefficients R_c, which are 0.327, 0.239, and 0.254. Fig. 8 shows the comparison between the Cs-137 observations and model predictions using the recovered release rates from case R01 and R02. Because the Cs-137 concentrations are plotted on a logarithmic scale, the apparent linear relationship between observations and model results actually reflect their $ln(c)$-based correlations. Correspondingly, observations and simulated Cs-137 concentrations using Katata et al. (2014), shown in Fig. 4 on a logarithmic scale scatter plot as well, have a $ln(c)$-based correlation of $R_{ln(c)} = 0.376$ and a concentration-based correlation coefficient $R_c = 0.255$. In alleviating the original extreme over- or under-estimation for some samples, the release rates are adjusted to have improved agreements between the measurements and simulations when measured by $R_{ln(c)}$.

4.2. Observation availability

Without the inherent model uncertainties associated with the long range transport and deposition, accurate local and regional measurements close to the source are the preferred data for the inverse modeling. However, these data are not always available, or at least not in a timely matter, while some global networks, such as air concentrations from the IMS of CTBT provide reliable and near-real-time observations. In this section, we will test whether using only a subset of the observations still permits the quantification of temporal variations of emissions from a known source location.

Each group of data listed in Table 1, i.e., CTBT, EPAR, EURO, and EXTR, are assimilated into the inverse modeling system separately in four cases, R04-07. The description of the cases are listed in Table 4. Except for the assimilated data, cases R05-07 are otherwise same as R02. To ensure that the smoothness term will not dominate the cost function, the final $\mathscr{J}_{sms}/\mathscr{J}_{total}$ values are also listed in Table 4. They have a range of 0.012–0.053 for cases R02-07.

Fig. 9 shows that R04, R06, and R07 all have the highest peak release value on March 18, similar to those estimated by R02. With the most observations assimilated, the release estimates of Case R06 using the EURO data nearly have a perfect match with the 96-h Katata et al. results from March 16 to March 23. Its overall statistics for the release rates are similar to case R02 that assimilates all observations, with MRE = 1.91 and a correlation coefficient R = 0.671, as listed in Table 5. The release rate statistics are only slightly worse for case R07, with MRE = 2.09 and a correlation coefficient R = 0.668. Fig. 9 shows that the estimated emissions of R07 agree well with the 96-h Katata et al. results, although the peak value on March 18 is lower. Case R04 with CTBT data has similar Cs-137 release estimates as R07 does until March 21, when it starts to deviate from the Katata et al. results. Table 5 shows that its release rate MRE = 4.69, which is more than twice of those for cases R06 and R07. The release correlation coefficient is also much lower at R = 0.464. Compared to R04, the relatively better release estimates of case R07 are probably due to the fact that the model predictions have less biases on the EXTR data when using the Katata et al. (2014) release estimates, shown in Figs. 4 and 6.

Among cases R04-07, case R05 that assimilates EPAR data has the worst performance in estimating the emission rates. It is because the current EPAR data do not have April observations

Table 5
Evaluation statistics of Cs-137 concentrations and recovered releases, q, for cases using actual Cs-137 measurements. The statistics for q are obtained by assuming Katata et al. (2014) estimates as the "true" solutions. For cases R04-06, the Cs-137 concentration statistics calculation only includes the measurements assimilated. MAE: mean absolute error; RMSE: root-mean-square error; MRE: mean relative error; R: linear correlation coefficient. Units of MAE and RMSE: mBq/m^3 for concentrations, Bq/h for releases.

Case	Cs-137 concentration					Cs-137 release			
	MAE	RMSE	MRE	R_c	$R_{ln(c)}$	MAE	RMSE	MRE	R
R01	0.158	0.591	3.508	0.327	0.518	$25.7 \cdot 10^{12}$	$55.0 \cdot 10^{12}$	2.96	0.444
R02	0.183	0.882	4.288	0.239	0.405	$12.4 \cdot 10^{12}$	$22.0 \cdot 10^{12}$	1.96	0.674
R03	0.182	0.824	3.770	0.254	0.425	$13.9 \cdot 10^{12}$	$24.7 \cdot 10^{12}$	1.77	0.631
R04	0.293	1.110	3.505	0.235	0.562	$17.5 \cdot 10^{12}$	$26.1 \cdot 10^{12}$	4.69	0.464
R05	0.853	1.351	11.305	0.053	0.150	$26.5 \cdot 10^{12}$	$35.0 \cdot 10^{12}$	11.35	0.231
R06	0.067	0.129	4.460	0.095	0.189	$12.4 \cdot 10^{12}$	$22.3 \cdot 10^{12}$	1.91	0.671
R07	0.192	0.649	1.179	0.543	0.449	$13.1 \cdot 10^{12}$	$23.1 \cdot 10^{12}$	2.09	0.668

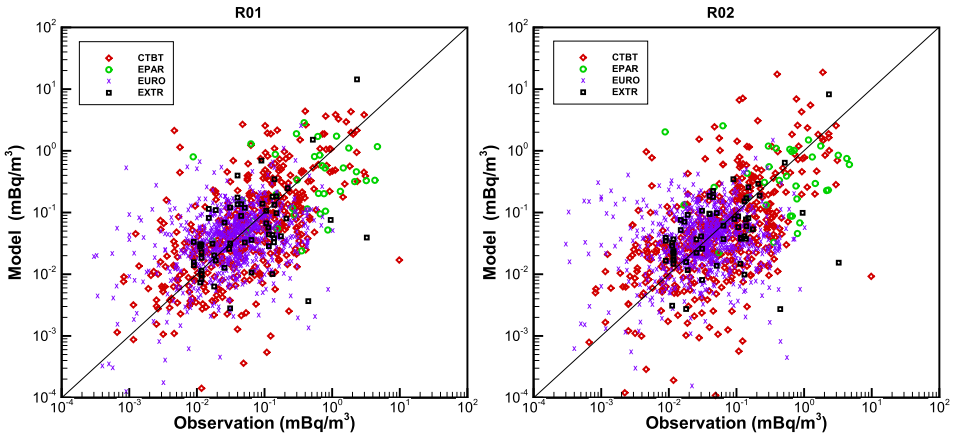

Fig. 8. Scatter plots of Cs-137 observations and model predictions using recovered release rates from case R01 (left) and R02 (right).

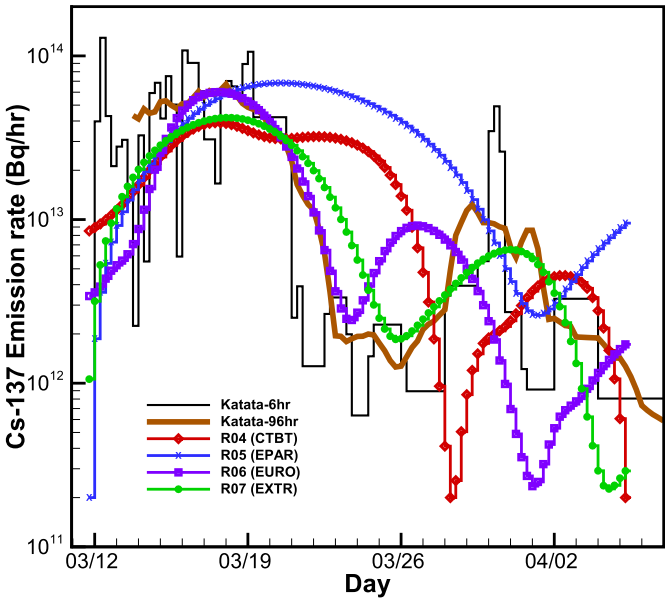

Fig. 9. Cs-137 release estimates from tests using the CTBT (R04), EPAR(R05), EURO (R06), and EXTR (R07) measurements. Cs-137 releases estimates by Katata et al. (2014) are also shown for comparison. Katata-96hr estimates are centered running averages based on the 6-hr results.

included. This makes it impossible to determine the release rates for most of the 99 6-hr segments, demonstrated by the limited extent of average H_{im} in time shown in Fig. 2.

5. Summary and discussion

An inverse emission estimation system based on a transfer coefficient matrix (TCM) created using the HYSPLIT Lagrangian dispersion model and a cost functional that measures the differences between the model predictions and the actual air concentration measurements is developed. The system is first tested with identical twin experiments, in which pseudo observations are generated with the same model used to estimate the transfer coefficients. With the pseudo observations generated at the same location and time as the actual Cs-137 observations to be assimilated later, the system is able to accurately recover the release rates and obtain better release estimates than the use of the singular value decomposition (SVD) method. It is found that using $ln(c)$ differences between model and observations in the cost functional achieves better results than using the original air concentration c differences. Using twin experiments with added noise to simulate the observational errors, the inverse estimation results are found to be robust and not overly sensitive to the first guess of the release.

When the actual cesium-137 air concentration measurements after the Fukushima nuclear accident are used to estimate the release of the radionuclide, a penalty term is added in the cost functional to create smooth temporal changes. While the temporal variations of the release rates at 6-h segments cannot be fully retrieved using 24-h observations, the features at larger time scales are well recovered. In tests where only some subsets of the available measurement data are assimilated, the system still manages to get main events identified in the estimated temporal profile of releases.

The source location is known for all the tests presented here. If the source location is unknown, the inverse emission estimation system can be applied by extending the control variables over space. Adding additional dimensions to the control variables will increase the number of the unknowns significantly. To successfully apply the inverse system, one will need a large amount of measurement data to estimate the emissions. In such applications, better *a priori* estimates may be crucial. In addition, a spatial smoothness penalty term might be needed as well. Further testing will be performed in the future.

Acknowledgments

This study was supported by NOAA grant NA09NES4400006 (Cooperative Institute for Climate and Satellites-CICS) at the NOAA Air Resources Laboratory in collaboration with the University of Maryland. Additional funding for this study was provided by the U.S. Department of State.

References

Achim, P., Monfort, M., Le Petit, G., Gross, P., Douysset, G., Taffary, T., Blanchard, X., Moulin, C., MAR 2014. Analysis of radionuclide releases from the Fukushima Dai-ichi nuclear power plant accident Part II. Pure Appl. Geophys. 171 (3–5), 645–667.

Auer, M., Prior, M.K., Sep. 2014. A new era of nuclear test verification. Phys. Today 67 (9), 39–44.

Becker, A., Wotawa, G., De Geer, L.-E., Seibert, P., Draxler, R.R., Sloan, C., D'Amours, R., Hort, M., Glaab, H., Heinrich, P., Grillon, Y., Shershakov, V., Katayama, K., Zhang, Y., Stewart, P., Hirtl, M., Jean, M., Chen, P., JUL 2007. Global backtracking of anthropogenic radionuclides by means of a receptor oriented ensemble dispersion modelling system in support of Nuclear-Test-Ban Treaty verification. Atmos. Environ. 41 (21), 4520–4534.

Chino, M., Nakayama, H., Nagai, H., Terada, H., Katata, G., Yamazawa, H., JUL 2011.

Preliminary estimation of release amounts of I-131 and Cs-137 accidentally discharged from the Fukushima Daiichi Nuclear Power Plant into the atmosphere. J. Nucl. Sci. Technol. 48 (7), 1129–1134.
Daley, R., 1991. Atmospheric Data Analysis. Cambridge University Press.
Draxler, R., Hess, G., December 1997. Description of the HYSPLIT_4 Modeling System. Tech. Rep. NOAA Technical Memo ERL ARL-224. National Oceanic and Atmospheric Administration, USA.
Draxler, R., Hess, G., December 1998. An overview of the HYSPLIT_4 modeling system for trajectories, dispersion and deposition. Aust. Meteor. Mag. 47 (4), 295–308.
Draxler, R., Rolph, G., McQueen, J., Heffter, J., Stunder, B., September 1993. Capabilities of the NOAA Washington regional specialized meteorological center for atmospheric transport model products for environmental emergency response. In: International Workshop on Users' Requirements for the Provision of Atmospheric Transport Model Products for Environmental Emergency Response. Montréal, Québec, Canada, p. 18.
Draxler, R.R., Rolph, G.D., 2012. Evaluation of the Transfer Coefficient Matrix (TCM) approach to model the atmospheric radionuclide air concentrations from Fukushima. J. Geophys. Res. 117, D05107.
Hirao, S., Yamazawa, H., Nagae, T., Feb 2013. Estimation of release rate of iodine-131 and cesium-137 from the Fukushima Daiichi nuclear power plant. J. Nucl. Sci. Technol. 50 (2), 139–147.
Katata, G., Chino, M., Kobayashi, T., Terada, H., Ota, M., Nagai, H., Kajino, M., Draxler, R., Hort, M.C., Malo, A., Torii, T., Sanada, Y., 2014. Detailed source term estimation of the atmospheric release for the Fukushima Daiichi nuclear power station accident by coupling simulations of atmospheric dispersion model with improved deposition scheme and oceanic dispersion model. Atmos. Chem. Phys. Discuss. 14 (10), 14725–14832.
Katata, G., Ota, M., Terada, H., Chino, M., Nagai, H., JUL 2012. Atmospheric discharge and dispersion of radionuclides during the Fukushima Dai-ichi Nuclear Power Plant accident. Part I: source term estimation and local-scale atmospheric dispersion in early phase of the accident. J. Environ. Radioact. 109, 103–113.
Kleist, D.T., Parrish, D.F., Derber, J.C., Treadon, R., Wu, W.-S., Lord, S., DEC 2009. Introduction of the GSI into the NCEP global data assimilation system. Weather Forecast. 24 (6), 1691–1705.
Kobayashi, T., Nagai, H., Chino, M., Kawamura, H., OCT 1 2013. Source term estimation of atmospheric release due to the Fukushima Dai-ichi Nuclear Power Plant accident by atmospheric and oceanic dispersion simulations. J. Nucl. Sci. Technol. 50 (3), 255–264.
Lin, C.-L., Chai, T., Sun, J., 2002. On smoothness constraints for four-dimensional data assimilation. J. Comput. Phys. 181, 430–453.
Maryon, R.H., Ryall, D.B., Malcolm, A.L., 1999. The NAME 4 Dispersion Model: Science Documentation. Tech. Rep. Turbulence Diffusion Note No. 262, UK Meteorological Office.
Masson, O., Baeza, A., Bieringer, J., Brudecki, K., Bucci, S., Cappai, M., Carvalho, F.P., Connan, O., Cosma, C., Dalheimer, A., Didier, D., Depuydt, G., De Geer, L.E., De Vismes, A., Gini, L., Groppi, F., Gudnason, K., Gurriaran, R., Hainz, D., Halldorsson, O., Hammond, D., Hanley, O., Holey, K., Homoki, Z., Ioannidou, A., Isajenko, K., Jankovic, M., Katzlberger, C., Kettunen, M., Kierepko, R., Kontro, R., Kwakman, P.J.M., Lecomte, M., Vintro, L.L., Leppanen, A.-P., Lind, B., Lujaniene, G., Mc Ginnity, P., Mc Mahon, C., Mala, H., Manenti, S., Manolopoulou, M., Mattila, A., Mauring, A., Mietelski, J.W., Moller, B., Nielsen, S.P., Nikolic, J., Overwater, R.M.W., Palsson, S.E., Papastefanou, C., Penev, I., Pham, M.K., Povinec, P.P., Rameback, H., Reis, M.C., Ringer, W., Rodriguez, A., Rulik, P., Saey, P.R.J., Samsonov, V., Schlosser, C., Sgorbati, G., Silobritiene, B.V., Soderstrom, C., Sogni, R., Solier, L., Sonck, M., Steinhauser, G., Steinkopff, T., Steinmann, P., Stoulos, S., Sykora, I., Todorovic, D., Tooloutalaie, N., Positti, L., Tschiersch, J., Ugron, A., Vagena, E., Vargas, A., Wershofen, H., Zhukova, O., SEP 15 2011. Tracking of airborne radionuclides from the damaged Fukushima Dai-ichi Nuclear Reactors by European networks. Environ. Sci. Technol. 45 (18), 7670–7677.
Oza, R.B., Indumati, S.P., Puranik, V.D., Sharma, D.N., Ghosh, A.K., AUG 2013. Simplified approach for reconstructing the atmospheric source term for Fukushima Daiichi nuclear power plant accident using scanty meteorological data. Ann. Nucl. Energy 58, 95–101.
Press, W.H., Flannery, B.P., Teukolsky, S.A., Vetterling, W.T., 1986. Numerical Recipes: the Art of Scientific Computing. Cambridge University Press, New York.
Rolph, G., McQueen, J., Draxler, R., 1-3 September 1993. Real-time environmental applications and display system (READY). In: Topical Meeting on Environmental Transport and Dosimetry. American Nuclear Society, Charleston, SC, USA, pp. 113–116.
Saunier, O., Mathieu, A., Didier, D., Tombette, M., Quelo, D., Winiarek, V., Bocquet, M., 2013. An inverse modeling method to assess the source term of the Fukushima Nuclear Power Plant accident using gamma dose rate observations. Atmos. Chem. Phys. 13 (22), 11403–11421.
Schöeppner, M., Plastino, W., Povinec, P.P., Wotawa, G., Bella, F., Budano, A., De Vincenzi, M., Ruggieri, F., DEC 2012. Estimation of the time-dependent radioactive source-term from the Fukushima nuclear power plant accident using atmospheric transport modelling. J. Environ. Radioact. 114 (SI), 10–14.
Sportisse, B., APR 2007. A review of parameterizations for modelling dry deposition and scavenging of radionuclides. Atmos. Environ. 41 (13), 2683–2698.
Stohl, A., Seibert, P., Wotawa, G., Arnold, D., Burkhart, J.F., Eckhardt, S., Tapia, C., Vargas, A., Yasunari, T.J., 2012. Xenon-133 and caesium-137 releases into the atmosphere from the Fukushima Dai-ichi nuclear power plant: determination of the source term, atmospheric dispersion, and deposition. Atmos. Chem. Phys. 12 (5), 2313–2343.
Tanabe, F., 2012. A scenario of large amount of radioactive materials discharge to the air from the unit 2 reactor in the Fukushima Daiichi NPP accident. J. Nucl. Sci. Technol. 49 (4), 360–365.
Terada, H., Katata, G., Chino, M., Nagai, H., OCT 2012. Atmospheric discharge and dispersion of radionuclides during the Fukushima Dai-ichi Nuclear Power Plant accident. Part II: verification of the source term and analysis of regional-scale atmospheric dispersion. J. Environ. Radioact. 112, 141–154.
Winiarek, V., Bocquet, M., Duhanyan, N., Roustan, Y., Saunier, O., Mathieu, A., JAN 2014. Estimation of the caesium-137 source term from the Fukushima Daiichi nuclear power plant using a consistent joint assimilation of air concentration and deposition observations. Atmos. Environ. 82, 268–279.
Winiarek, V., Bocquet, M., Saunier, O., Mathieu, A., MAR 9 2012. Estimation of errors in the inverse modeling of accidental release of atmospheric pollutant: application to the reconstruction of the cesium-137 and iodine-131 source terms from the Fukushima Daiichi power plant. J. Geophys. Res. Atmos. 117.
Zhu, C., Byrd, R.H., Lu, P., Nocedal, J., 1997. L-BFGS-B–fortran subroutines for large scale bound constrained optimization. ACM Trans. Math. Softw. 23 (4), 550–560.